Non-linear finite-element analysis of prestressed concrete members

S. M. Seraj, BScEng, MScEng, DIC, PhD, M. D. Kotsovos, Dipl(Eng), DIC, PhD, DSc, MIStructE, and M. N. Pavlović, BEng, MEngSc, PhD

Proc. Instn Civ. Engrs Structs & Bldgs, 1992, **94**, Nov., 403–418

Paper 9885

Written discussion closes 15 January 1993

The generality of a recently developed 'constant parameter' three-dimensional finite-element model for structural concrete, based on a brittle constitutive relationship at the material level, is now extended to prestressed concrete members. The adopted technique of applying the prestressing force as a constant load at the first load step of the non-linear analysis, and removing from the input that part of the steel tendon stress–strain curve which is effectively utilized in the prestressing operation, although somewhat simplistic, is found to be adequate for practical purposes. What emerges from the present Paper is that the existing finite-element package, applied in the past to plain and/or reinforced concrete members made from a wide range of concrete strengths, is equally capable of catering for prestressed concrete structural forms. As well as serving as a tool for analysis, the numerical model also provides insight into design itself by identifying the path of the compressive forces within a structure.

Notation

a	shear span
d	effective depth
f_c	uniaxial compressive strength of 100 × 250 mm concrete cylinders
f'_c	uniaxial compressive strength of 6 × 12 in (150 × 300 mm) concrete cylinders
f_y	yield strength of reinforcement; a stress equivalent to 1% strain in prestressing tendon
f_u	ultimate strength of prestressing tendon
$f_{y,\,model}$	$f_y - \sigma_p$
$f_{u,\,model}$	$f_u - \sigma_p$
σ_p	stress in prestressing tendon due to effective prestressing

Introduction

A fully three-dimensional (3-D) finite-element (FE) package for reinforced-concrete (RC) structural forms,[1] requiring only the British standard cylinder strength f_c for material input, has recently been developed, its wide-ranging applicability having been proven on the basis of several case studies of varying complexities[2,3] and concrete strengths.[4] The present Paper aims at extending the generality of the 3-D model so as to encompass also prestressed-concrete (PSC) members through the introduction of simple techniques in the input for the prestressing steel. The results also provide information on the possible influence of the path through which compressive forces are transmitted in a PSC beam on the design of such members. Throughout this study, the recommendations for the non-linear strategy to be followed and the plotting convention are as outlined in references 1–3.

Modelling of PSC members

2. The effect of prestressing in a PSC member is to induce initial stresses in the concrete and reinforcing steel. When using the present model for the analysis of PSC structures, stresses in the concrete can be simulated by applying the total effective prestressing force on the structural member right at the first load step so that, in the subsequent load steps of the non-linear analysis, only the increments of the non-prestressing applied forces are considered (as for RC members). On the other hand, the proposed modelling of the prestressing tendon can best be explained with reference to Fig. 1, in which the stress–strain relationship of a typical prestressing strand has been shown diagrammatically. Owing to the absence of a real yield stress value in a prestressing tendon, a stress equivalent to 1% strain has been conveniently chosen as the yield stress f_y. If f_u is considered as the ultimate stress of the tendon, and σ_p as the stress up to which the tendon is stressed after all the losses have taken place, it is sensible to use the values of $(f_y - \sigma_p)$ and $(f_u - \sigma_p)$ as inputs of $f_{y,\,model}$ and $f_{u,\,model}$ respectively. Thus, it is proposed that, by removing the part of the stress–strain curve used during the prestressing operation from the actual stress–strain curve of the tendon, and by using this modified stress–strain curve as input in the FE model, the effects of the prestressing force in the tendon can be represented without the more formal inclusion of initial stresses and strains.

Investigation programme

3. As is well known, faithful numerical simulation of an experimental finding is heavily dependent upon the availability of all the relevant experimental details. The applicability of the present 3-D FE model to PSC members has been tested on the basis of a set of four experimental case studies conducted on both I-beams and T-beams and an additional

S. M. Seraj, Imperial College of Science, Technology and Medicine, University of London

M. D. Kotsovos, National Technical University of Athens

M. N. Pavlovic, Imperial College of Science, Technology and Medicine, University of London

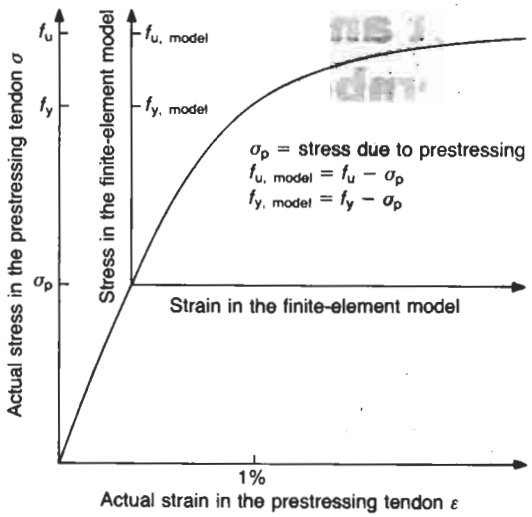

Fig. 1. Stress–strain diagram for prestressing tendon

case study of a purely numerical nature. While the pertinent technicalities of case study 1 are available elsewhere,[5,6] the Authors performed the actual laboratory tests on the other three case studies. The PSC members analysed in this Paper differ in the amount of prestressing, loading arrangement, geometry and reinforcement detailing. During the simulation exercise, those parameters of direct interest to the designer—namely the failure load, deformation response and cracking process—have been compared with their experimental counterparts for each of the first four case studies. (Owing to space limitations, mention of experimental cracking patterns has been limited to case studies 1 and 2; a fuller picture of the relevant information for case studies 2, 3 and 4 is available in reference 7.) The fifth case study, a numerical experiment on a PSC T-beam made from a high-strength concrete (HSC) mix is also included as probably the first of its kind ever reported. To facilitate comparison of crack patterns and deformations among the various case studies, the figures for these have been grouped together (Figs 2 and 3 respectively).

Case study 1. I-beam subjected to two-point loading failing in web shear

4. The structural element under examination is a pre-tensioned PSC beam with an I-section, reinforced with both prestressing and non-prestressing reinforcing bars, and reported as CW12 by Elzanaty *et al.*[5,6] The cross-sectional characteristics and transverse reinforcement details of the beam are given in Fig. 4. However, the exact position of the reinforcing bars—and hence of the effective depth—cannot be determined from this figure without scaled measurement. The prestressing reinforcement was made up of 4–0·6 in (15 mm) dia. low-relaxation seven-wire ASTM Grade 270 strands. The area of each wire was 0·22 in^2 (141·93 mm^2). The stress at 1% extension was 253·55 ksi (1748·67 MPa) and the ultimate stress was 268·09 ksi (1848·95 MPa). Two types of non-prestressing reinforcing bar were used: deformed ASTM Grade 60, having an actual yield stress of 63 ksi (434 MPa) for the longitudinal reinforcement and stirrups of $\frac{3}{8}$ in (9·5 mm) dia.; and smooth round bars of 0·25 in (6·3 mm) dia., having a yield stress of 55 ksi (379 MPa), for the top reinforcement. The concrete cylinder strength for this beam was 5800 psi (40 MPa), while it was prestressed by an effective prestressing force of 96·8 kip (430·56 kN). On account of the small web thickness, single-legged stirrups at 10 in (254 mm) spacing were used. The portion of such reinforcement in the flange was arranged alternately, as can be seen from Fig. 4. The beam was loaded by two-point loading, with a shear span to depth ratio a/d equal to 3·75 (see reference 5, although in reference 6 the a/d is given

Fig. 2 (below and facing page). Crack patterns at various load levels up to failure (DM N = displacements magnified N times): (a) beam CW12 (DM 5); (b) beam PCB1 (DM 1); (c) beam PCB3 (DM 1); (d) beam PCB6 (DM 1, except for load step 777 where the actual deflections have been reduced by 50%); (e) beam PCB7 (DM 1)

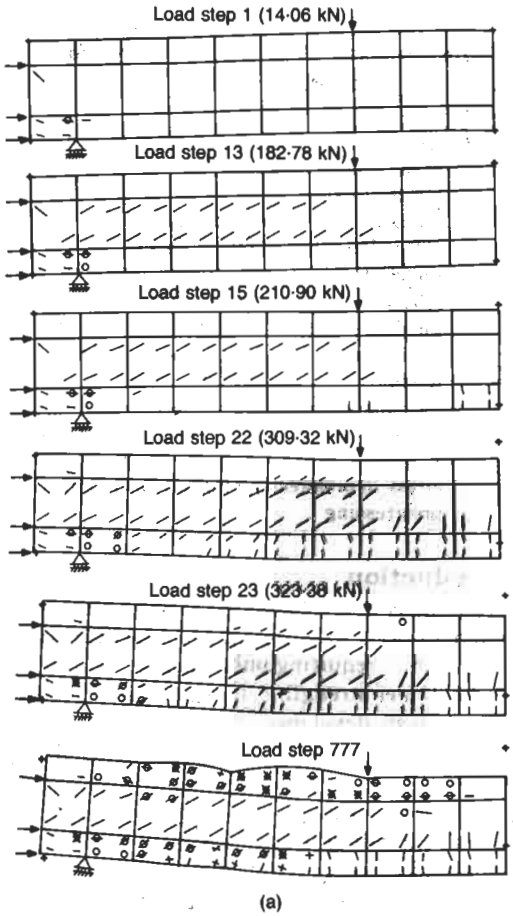

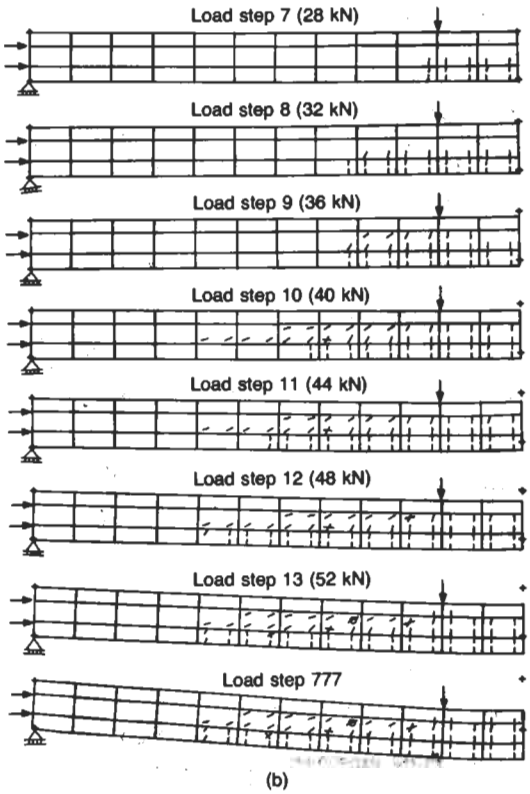

Fig. 2—continued

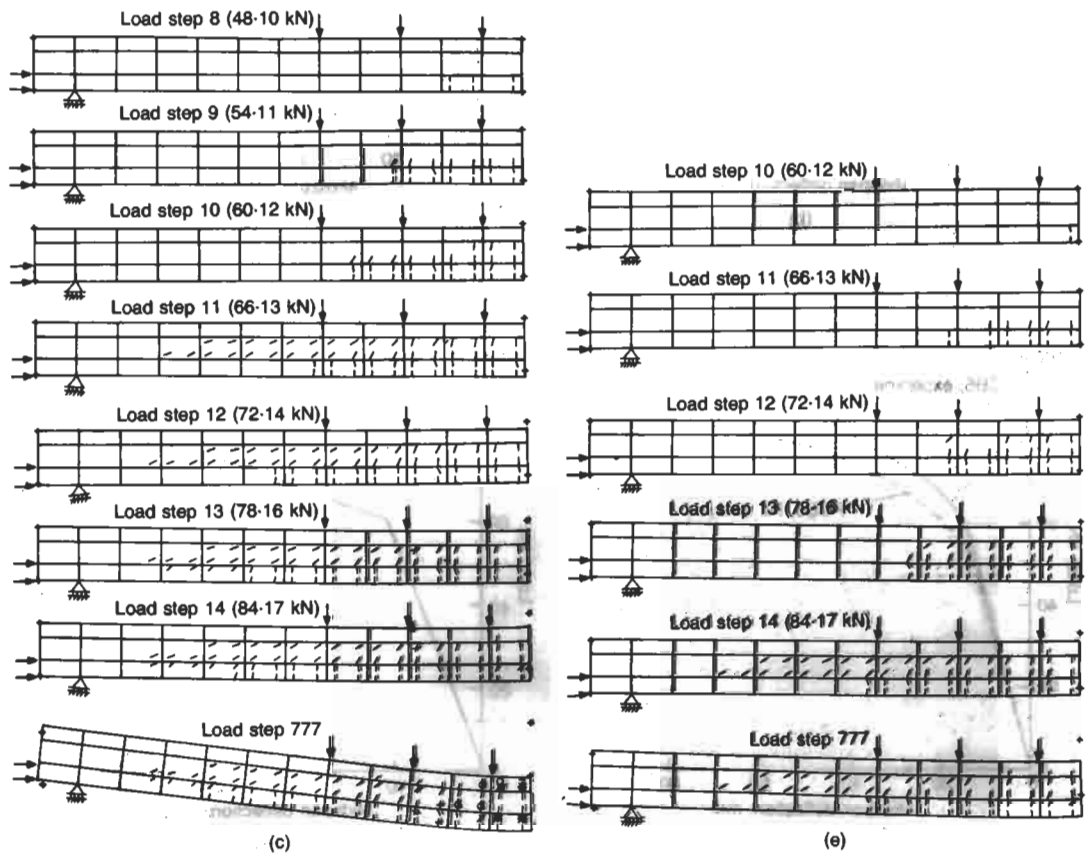

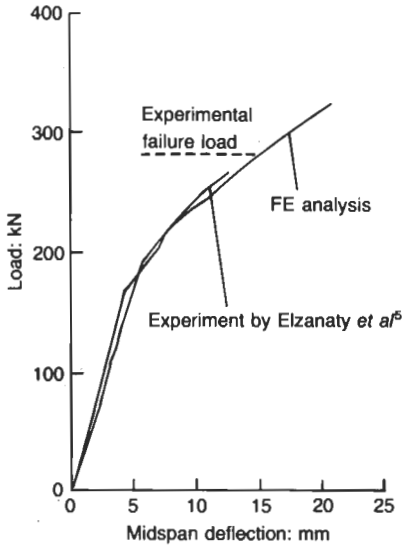

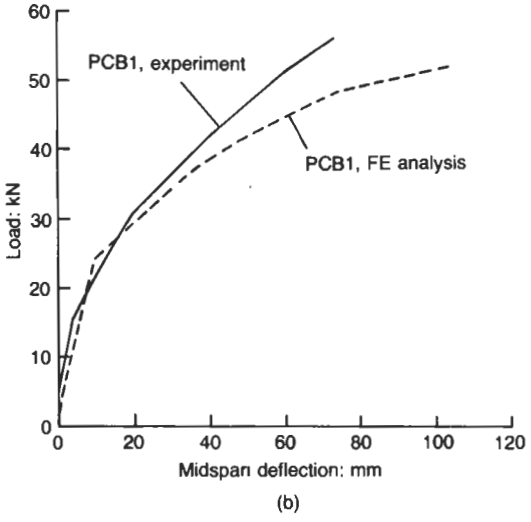

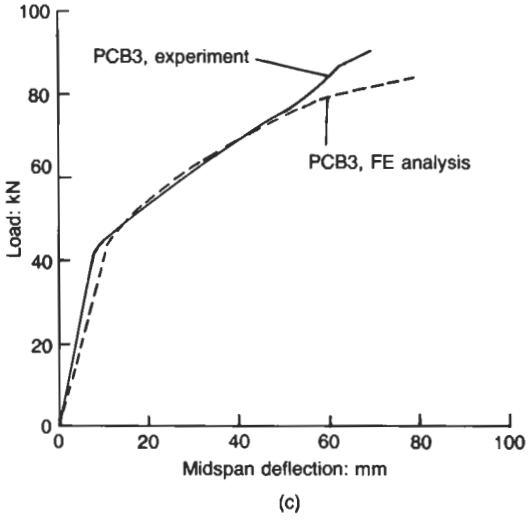

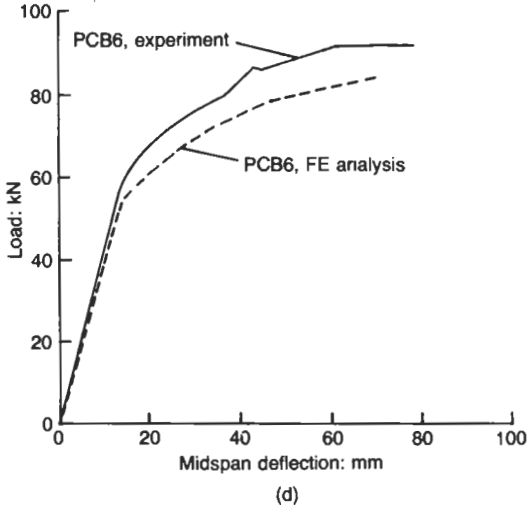

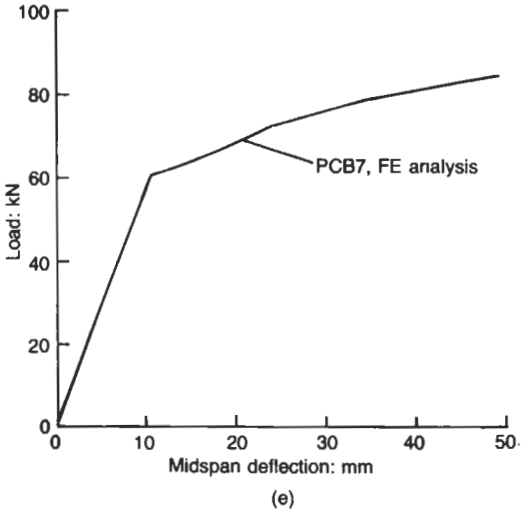

Fig. 3. Comparison between the experimental and the analytical load–deflection curves: (a) beam CW12; (b) beam PCB1; (c) beam PCB3; (d) beam PCB6; (e) beam PCB7

as 3·8). The loads for the onset of diagonal cracking and ultimate failure for this beam were 170·8 kN and 281·1 kN respectively.

5. The details of the FE mesh are shown in Fig. 5. The mesh comprises 50 brick elements for the concrete, and 192 bar elements for the steel. It is important to note that, in the strictest sense, the transverse reinforcement is not symmetric across the longitudinal axis of the beam as, in reality, it alternates from one side of the cross-section to the other (see Fig. 4). However, for practical purposes it can be averaged, and hence considered as symmetric; as a result, only one-fourth of the beam has been discretized on the basis of the assumed symmetry. Fig. 5 also indicates the area of reinforcement of the various steel elements of the mesh. The prestressing and non-prestressing steel elements were treated separately. The former were 'smeared' to the adjoining brick element edges in such a manner that the point of application of the resultant prestressing force remained unchanged. For purposes of estimating the length of the shear span, the distance of the centroid of the prestressing steel from the compression face has been considered as the effective depth (in the absence of explicit values in references 5 and 6). The effective prestressing stress σ_p was equal to 758·38 MPa. After subtracting the value of σ_p from the stress–strain curve of the tendon, the $f_{y,\,model}$ and $f_{u,\,model}$ for the FE input were found to be equal to 990·29 MPa and 1090·57 MPa respectively. The non-prestressing steel area was also 'smeared' to its adjacent nodes in a similar manner. The compression reinforcement was placed at the top edge of the beam and was discontinued in the flexural span. The main modification introduced in the modelling of the shear reinforcement was that the original one-legged alternately-placed stirrups were replaced by equivalent two-legged stirrups to introduce symmetry across the longitudinal direction; however, the total area of steel per unit length (in both the web and the flanges) was kept the same as in the actual beam.

6. The prestressing force was applied at the end of the beam as a constant force acting on the outside nodes of the prestressing steel elements. The amount of prestressing force at different nodes was varied depending on the area of the prestressing steel, so as to have everywhere the resultant prestressing force of the right magnitude and position. The vertical point loads were placed considering a/d to be equal to 3·75.

7. The maximum sustained load in the analysis was 323·38 kN, which is 15% higher than the experimental failure load of 281·11 kN. The analytical results may be discussed with reference to Figs 2(a) and 3(a), which show the analytical crack patterns up to failure and a comparison of the analytical and experimental load–deflection curves respectively. Note that the experimental load–deflection curve, as obtained from reference 5, ends at a load 267·76 kN, although the actual reported failure load mentioned earlier was higher. At the first load step, in which the effective prestressing force was applied to the beam all at once, cracks appeared at the end block of the beam parallel to the direction of the prestressing force. The beam remained free from any flexural or shear cracks up to a load of 182·78 kN when, suddenly, web-shear cracks emerged

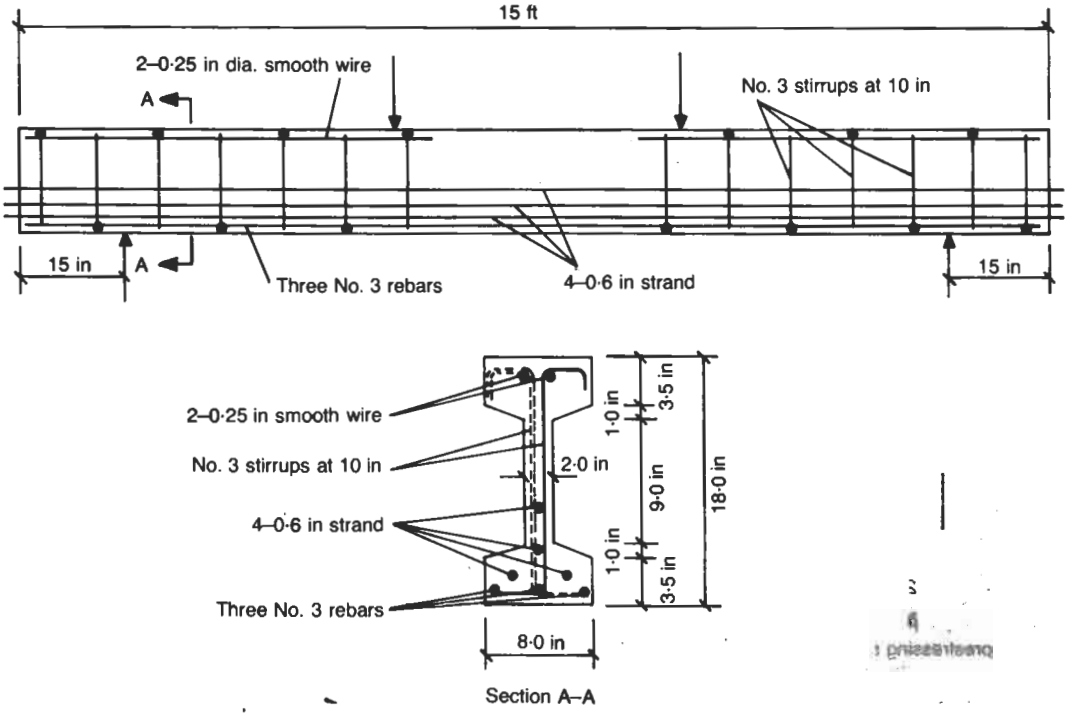

Fig. 4. Beam CW12: dimensions and reinforcement detailing

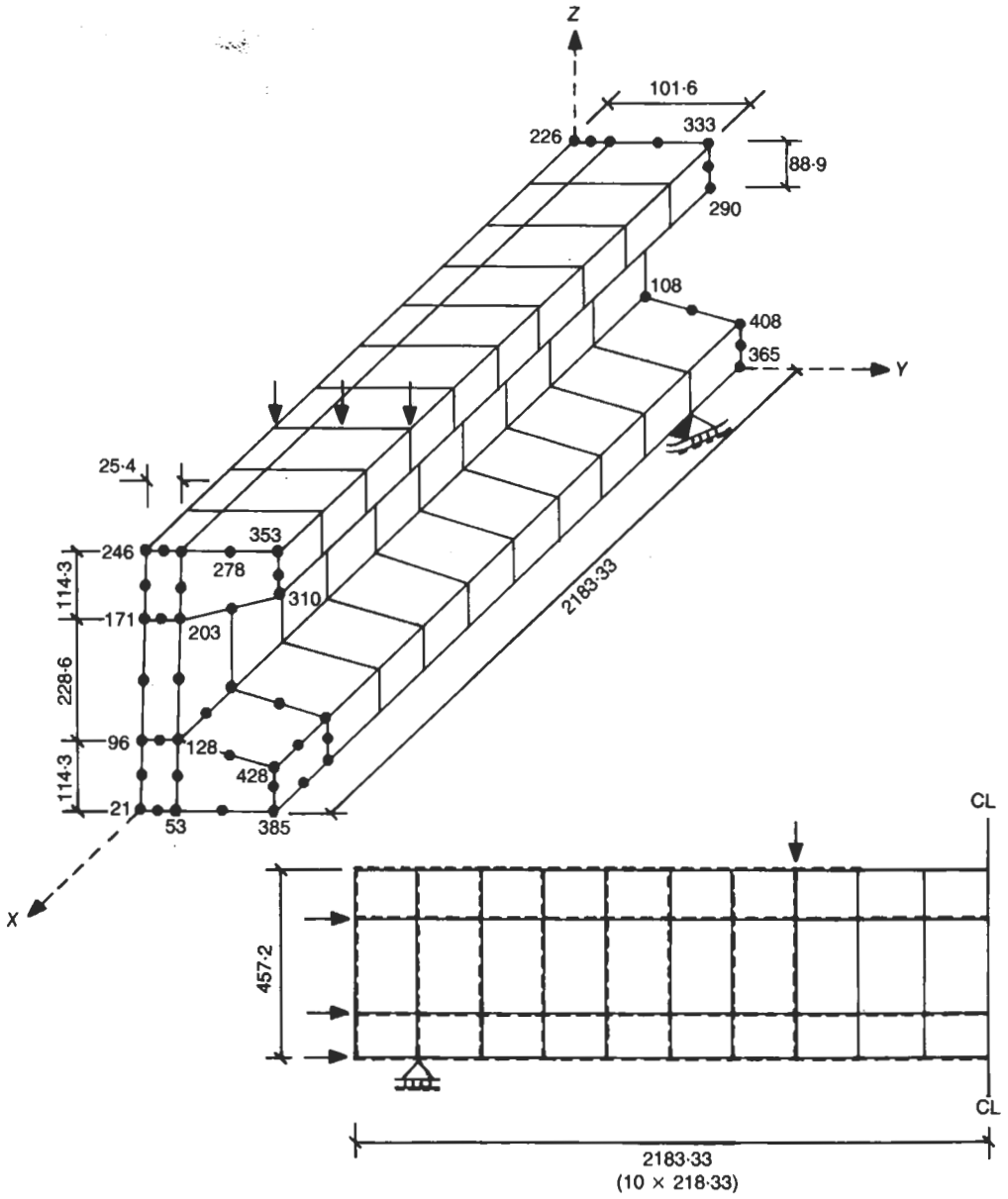

Fig. 5. Beam CW12: mesh of 50 HX20 brick elements (owing to symmetry, only one-fourth of the beam is analysed; the position of the steel elements is indicated by dashes) (all dimensions in mm)

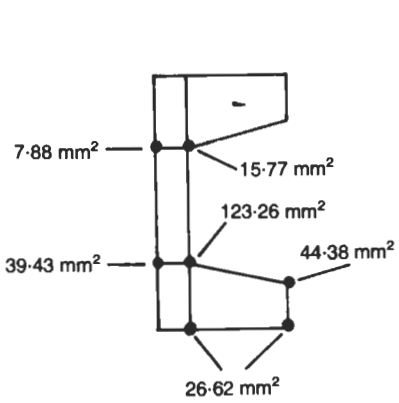

Position of
prestressing steel elements

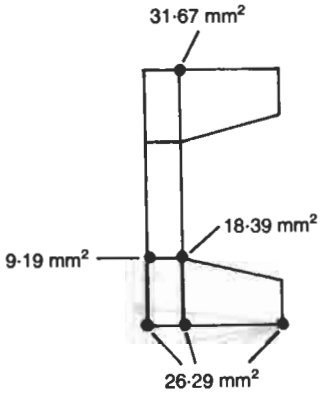

Position of
non-prestressing steel elements

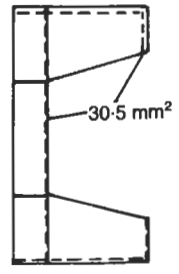

Position of
steel elements representing
shear reinforcement

along the whole length of the shear span. These cracks, which were formed at all the Gauss points of the web elements (making an angle of about 22·5° with the longitudinal direction of the beam), resembled quite well the cracks that formed during the experiment, at the diagonal-cracking load of 170·8 kN. At a total applied load of 210·9 kN, the first flexural cracks appeared in the middle of the flexural span and, also, just below the point load. One of the shear cracks extended towards the support at this stage. With the increase in load, flexural cracks were also formed in the shear span. At 309·3 kN, cracks near the loading points in the shear span started to propagate into the flange (hitherto uncracked) towards the actual point loads. At the maximum sustained load (MSL), additional cracks were formed in the top flange, defining more completely the compressive force trajectory. At this load step, a vertical crack (indicated by a circle) in the top flange near the point load was visible.

8. As can be seen from Fig. 3(a), the analytical load–deflection curve practically coincides with its experimental counterpart up to the experimental failure load, and then continues to follow a tangential path up to the MSL. This increased load sustainment in the analysis can be explained with reference to the modelling of the stirrups. In order to keep the computational efforts within the limit of available resources, symmetrical stirrups had to be introduced. In doing so, even though the total amount of reinforcement was carefully kept equal to the quantity used in the test, an additional confinement of the concrete was introduced in the analysis. It is important to note that even a small amount of confining pressure (of the order of 0·1 f_c) is sufficient to increase the load-carrying capacity of concrete by more than 50%.[8] Therefore, it is sensible to assume that, owing to the introduction of additional confinement in the FE analysis of CW12, the concrete in the compression zone sustained more load and, in turn, led the structural element to a higher failure load. Load step 777 of Fig. 2(a) supports this view regarding the confinement, as it shows that concrete in the top flange underwent a considerable amount of dilation at failure. In the test, owing to the presence of one-legged asymmetric stirrups, concrete (and thus the structural member) failed earlier, as concrete in the compression zone was not sufficiently confined. An additional reason for the numerical overestimate of the failure load is that the model used in the analysis relies greatly on the material properties. It should be stressed here that, in the input of the cylinder strength in the present FE analysis, the f'_c value of the American standard cylinder with the size 6 × 12 in was used instead of the f_c value of the British standard cylinder which has the size 100 × 250 mm (4 × 10 in). Now, Neville[9] reported that, for an increase in the height/diameter ratio from 2 to 2·5, the cylinder strength value of normal-strength concrete can decrease by about 10%. This reduction in f_c, if allowed for in the input of the FE model, would certainly have closed the gap between the analytical and experimental failure loads for the present case study. (A rerun with an f_c value of 36 MPa (= 0·9 f'_c) has, in fact, yielded an MSL of 309·32 kN, i.e. only 10% above the experimental failure load.) It is therefore evident from the analysis of case study 1 that even after adopting a crude and simplistic way of modelling the effects of prestressing (and reinforcement detailing) within the 3-D FE package, a satisfactory and realistic response can be achieved in the numerical simulation of PSC structural forms.

Case study 2. T-beam PCB1 subjected to two-point loading failing in shear

9. The cross-sectional characteristics and end-zone details of the post-tensioned PSC T-beams reported by Seraj[7]—referred to here as case studies 2 (PCB1), 3 (PCB3), 4 (PCB6) and 5 (PCB7)—are similar, and appear in Fig. 6. Beam PCB1, presently analysed, is a 6660 mm long girder, that is simply supported with a span of 6000 mm. The beam was subjected to a two-point loading with a shear span of 2500 mm. It is important to note here that, while the 5660 mm long PSC beams PCB3, PCB6 and PCB7 had the straight tendon profile depicted in Fig. 6, beam PCB1 possessed a slightly inclined tendon profile along a distance of 1000 mm from the end. The depth of the tendons at the prestressing and support levels were 150 mm and 178·84 mm (as measured from the top of the beam) respectively. Beam PCB1 was tested[7] in an effort to visualize the path through which the compressive force is transmitted in a PSC beam. The tendon profile of PCB1, along with the major crack pattern and the predicted compressive-force path (CFP), is shown in Fig. 7(a). It is worth mentioning here that the numerical modelling of the PSC T-beams reported in this Paper, coupled with the experimental findings of these and other PSC beams, led to the verification of a physical model proposed for the realistic design of PSC members.[7] While the experimental results and details of the physical model will be reported in future publications, it is imperative to mention here that, according to this model, provision of design transverse reinforcement only at locations where the CFP changes its direction (i.e. an area where the resultant of the prestressing force and the reaction meet the centroid of the uncracked compression zone) is sufficient to lead the PSC structural member to a ductile form of failure, provided that possible bond failure is prevented by placing additional

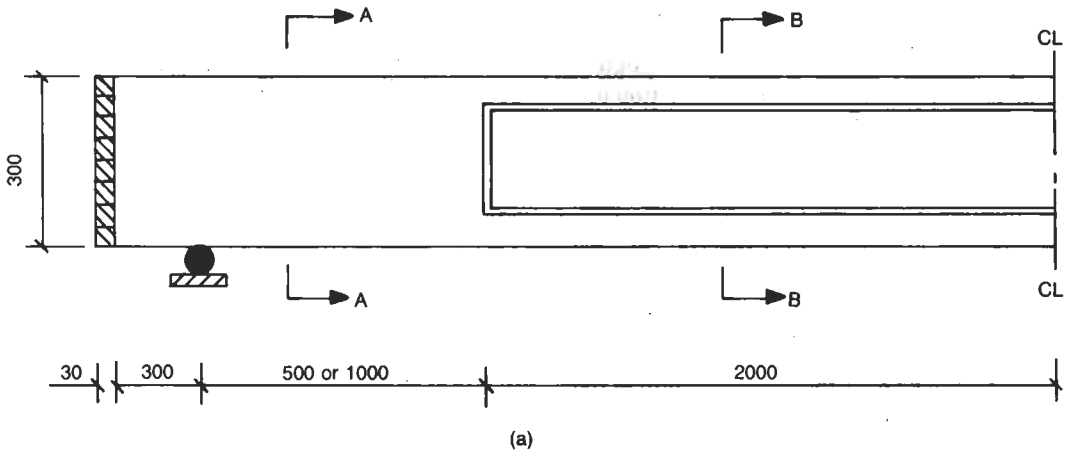

(a)

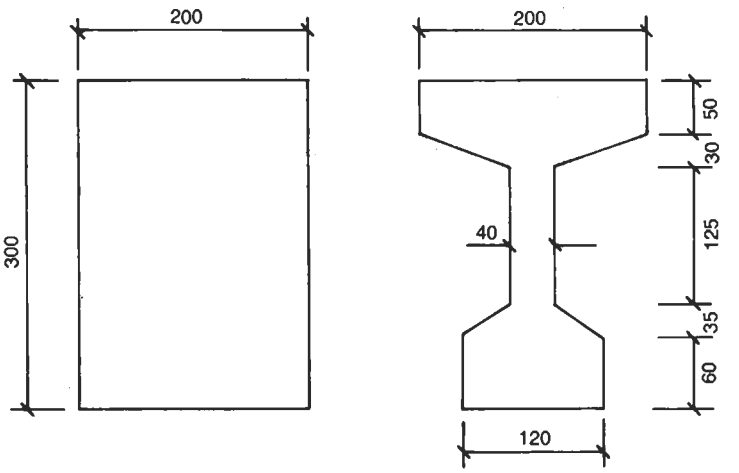

(b)

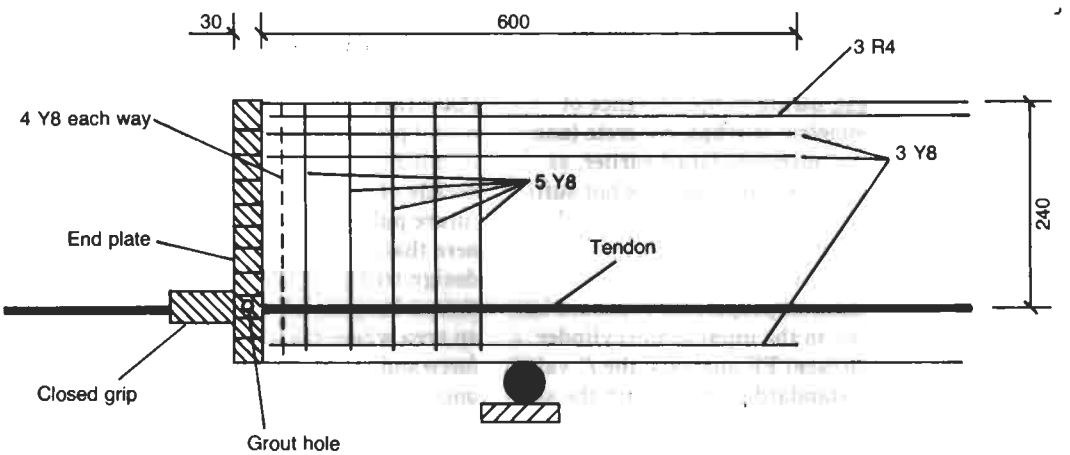

(c)

Fig. 6. (a) and (b) Cross-sectional characteristics; (c) typical reinforcement details of end zones of the PSC T-beams analysed (all dimensions in mm)

'hoop-like' reinforcement in the compression flange.

10. In order to test the basic ideas, the beam was neither designed to BS 8110,[10] nor were the recommendations of the CFP concept[11,12] implemented; such an approach ensured that the member would fail in shear, and therefore the web of the beam was furnished with nominal reinforcement. This nominal reinforcement was about 40% of the web reinforcement which is prescribed by BS 8110. On the other hand, this nominal web reinforcement could cater for only 60% of the transverse reinforcement (in accordance with the CFP design) needed at locations where the CFP changes its direction, in order to sustain the tensile force that develops at those places. In this way, while both the BS 8110 and the CFP design requirements refer to flexural failure, in the actual test[7] a shear type of failure was sought. However, in order to guarantee that the planned shear failure takes place as a result of the (additional) tensile stresses at the location where the CFP changes direction, and not as a result of bond failure, the flange of the beam was provided with an adequate amount of links, as can be calculated from CFP provisions. (The detailed calculation regarding the assessment of web and flange reinforcement, as advocated by BS 8110 and CFP methods for flexural failure of PCB1 to have occurred, is available elsewhere.[7])

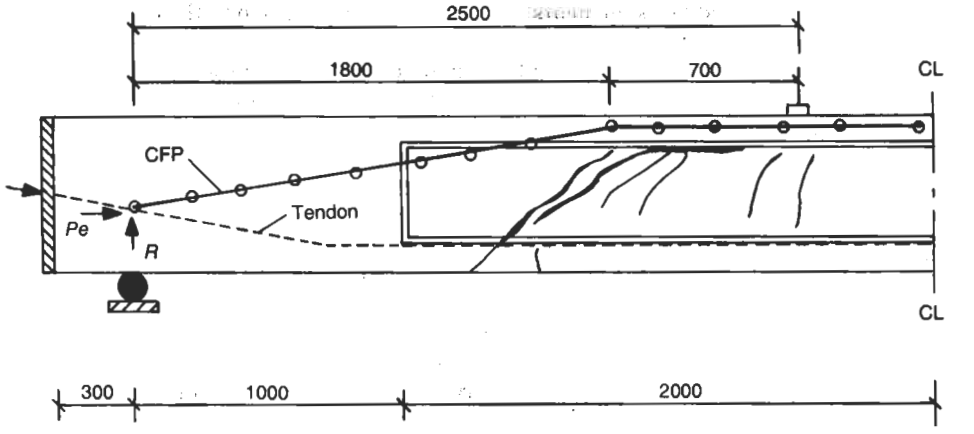

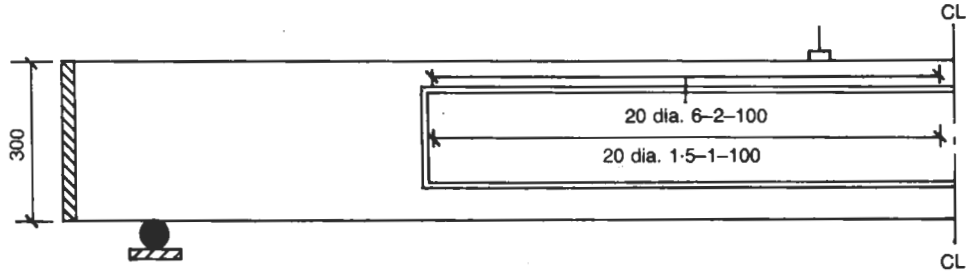

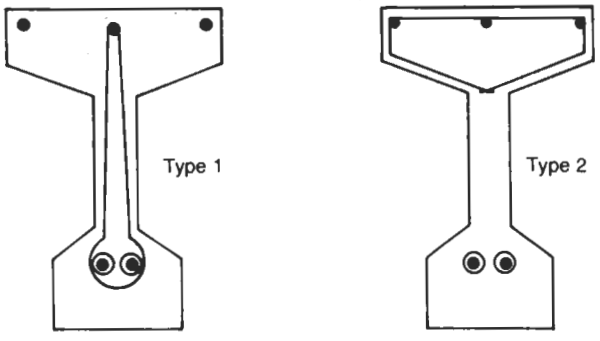

Fig. 7. Beam PCB1: (a) tendon profile, main crack pattern at failure, and CFP; (b) transverse reinforcement details (all dimensions in mm)

11. Beam PCB1 had two types of transverse reinforcement. Type 1 consisted of 1·5 mm dia. two-legged links extending from the top face of the beam to the level of the tension reinforcement, placed throughout that length of the beam having a T-section, at 100 mm spacing. Type 2 reinforcement comprised 6 mm dia. links placed around the top flange of the beam (again, throughout the T-section) at a spacing of 100 mm. Details of the transverse reinforcement are shown in Fig. 7(b). The strength characteristics of the tendons and reinforcing bars used in the PSC T-beams analysed in this Paper are listed in Table 1. The f_c value for PCB1 was 46·4 MPa.

12. The FE discretization adopted for the present analysis is given in Fig. 8. The mesh has 56 HX20 under-integrated brick elements for concrete and 182 LM03 bar elements for the steel (considering only one-fourth of the beam). A few minor simplifications were adopted during the discretization process. The bottom flange of the T-section of the beam was replaced by a trapezoidal section, thus saving 12 brick elements. Such a step can be justified on the basis of an earlier investigation,[4] which showed quite conclusively that, in the modelling of RC T-beams made from a wide range of concrete strengths, such a deviation from the actual shape of the bottom flange in the FE discretization has no impact on the overall prediction of the analysis. In fact, this type of slight modification in the geometry (essentially, a reduction in the area) of a structural form below the neutral axis is not expected to make an appreciable difference in the analytical predictions, as this is in keeping with the notion—propounded by the Authors—that cracked concrete in regions subjected to predominantly tensile-stress conditions (such as zones below the neutral axis) makes only a minor contribution to the overall load-carrying capacity of a concrete structure.[3] The rectangular section forming the end part of the beam, however, was properly discretized. On the other hand, the part of the beam beyond the support was omitted in the FE analysis, since the length of the member was quite large and hence the number of finite elements was high. (In case studies 3, 4 and 5, the smaller spans allow overhangs to be included in the FE analysis without impairing the economy of the runs.) The total amount of steel used in the end plate was lumped on to the edges at the support. More significant changes were made in the modelling of the prestressing tendon. Although the actual tendon profile was slightly inclined towards the end of the beam (see Fig. 7(a)), it was considered as a straight tendon; like the remainder of the tendon, it, too, was 'smeared' to the neighbouring brick-element edges. The effective prestressing force, however, was distributed at the nodes in such a manner that its resultant acted at the true tendon level at the support: as this force was 49% of the ultimate strength of the strands, the yield and ultimate strength of the tendon were inputted as 754·73 MPa and 978·63 MPa respectively (thus omitting that part of the stress–strain curve involved in the prestressing process). The area of the transverse reinforcement was adjusted so as to keep the same area per unit length as in the actual beam. The loading configuration adopted in the analysis was the same as in the experiment.

13. The analytical findings can be seen by reference to Figs 2(b) and 3(b), which give, respectively, crack patterns at various load levels up to failure and a comparison of the load–deflection curve with its experimental counterpart. As depicted in Fig. 2(b), the first set of flexural cracks was formed in the pure flexural span at an applied load of 28 kN. (Unlike beam CW12, analysed in case study 1, where end-zone cracking took place, the presence of the steel end-plate ensured that no such cracking due to prestressing occurred in PCB1.) In the next two load steps of 4 kN each, the number of flexural cracks increased and a few inclined cracks were formed. When the applied load reached 40 kN, that part of the web which consisted of a T-section was subjected to a large amount of diagonal cracking. All the flexural cracks reached the intersection of the top flange and the web at this stage. At a load of 44 kN, new cracks were formed in the bottom flange, and both the web and the bottom flange incurred additional cracking upon application of the next load step (48 kN). At the MSL level of 52 kN, which was about 92% of the experimental failure load of 57 kN, cracks entered into the top flange near the loading points. The crack patterns at the MSL and at the load step 777 are similar. If the symbols comprising either crosses or circle with oriented dash (i.e. doubly cracked zones), are connected by a hypothetical line, the cracking pattern at failure can be visualized; and from it, in turn, the location of the change in CFP trajectory may be estimated. This location where the CFP changes direction is marked by the Gauss point having a circle with a diagonal crack. It may be seen that numerical prediction of the crack

Table 1. Characteristics of reinforcing bars used in case studies 2–5

Type of reinforcement	f_y: MPa	f_u: MPa
12·9 mm dia. stabilized strand	1684·5	1908·5
6 mm dia. high yield steel	570	665
4 mm dia. mild steel	460	540
1·5 mm dia. mild steel	460	510

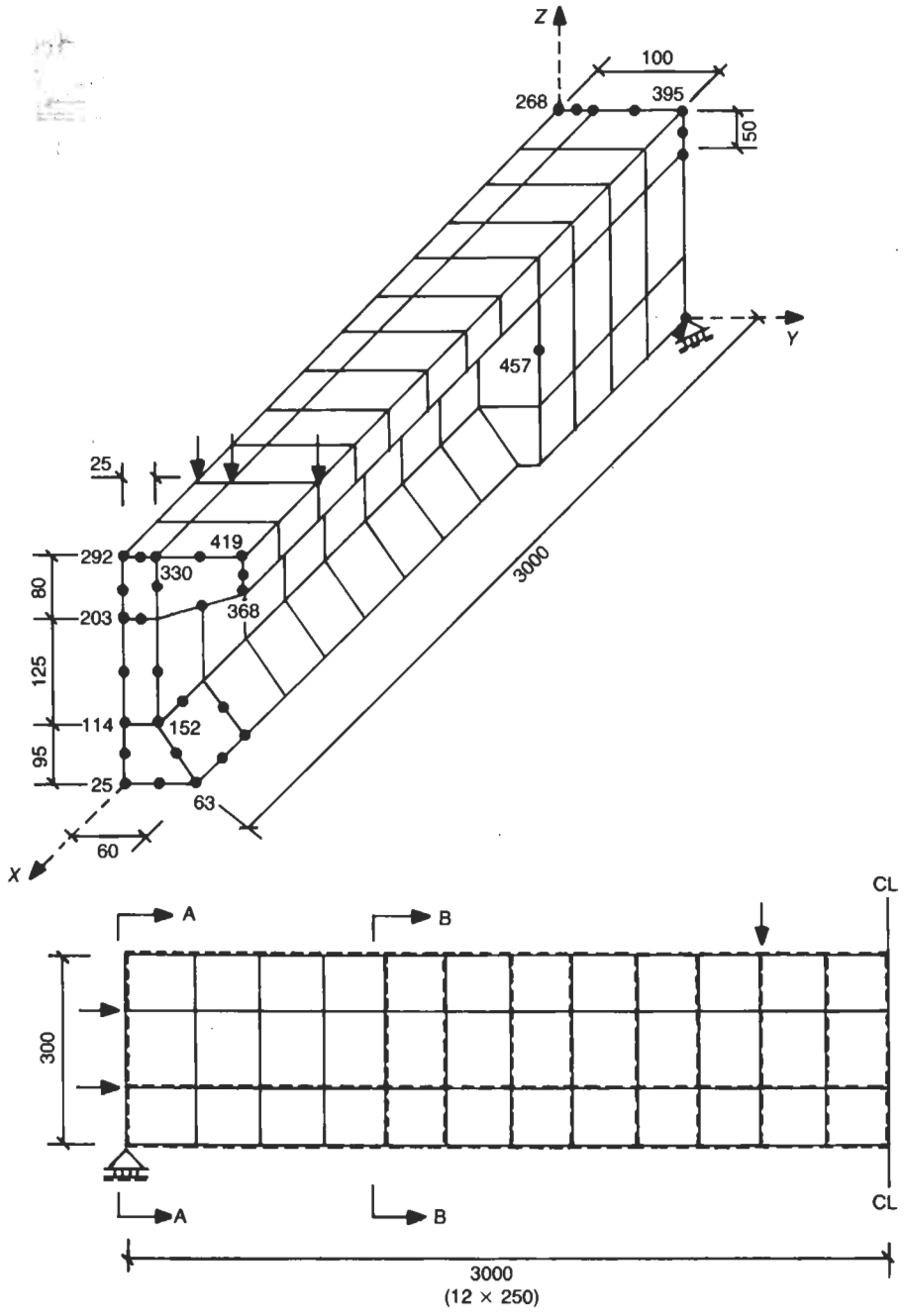

Fig. 8. Beam PCB1: mesh of 56 HX20 brick elements (owing to symmetry, only one-fourth of the beam is analysed; the position of the steel elements is indicated by dashes) (all dimensions in mm)

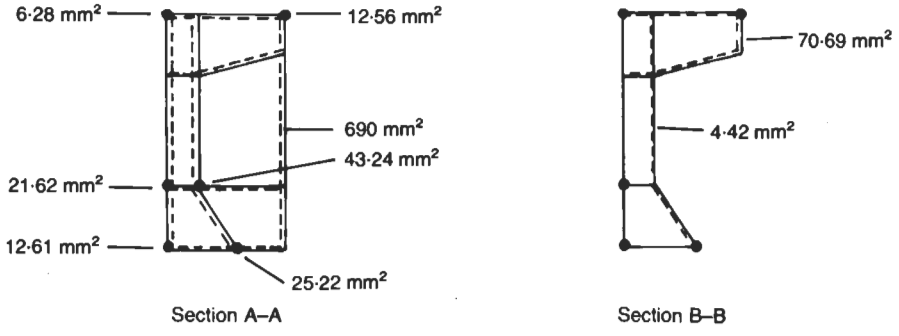

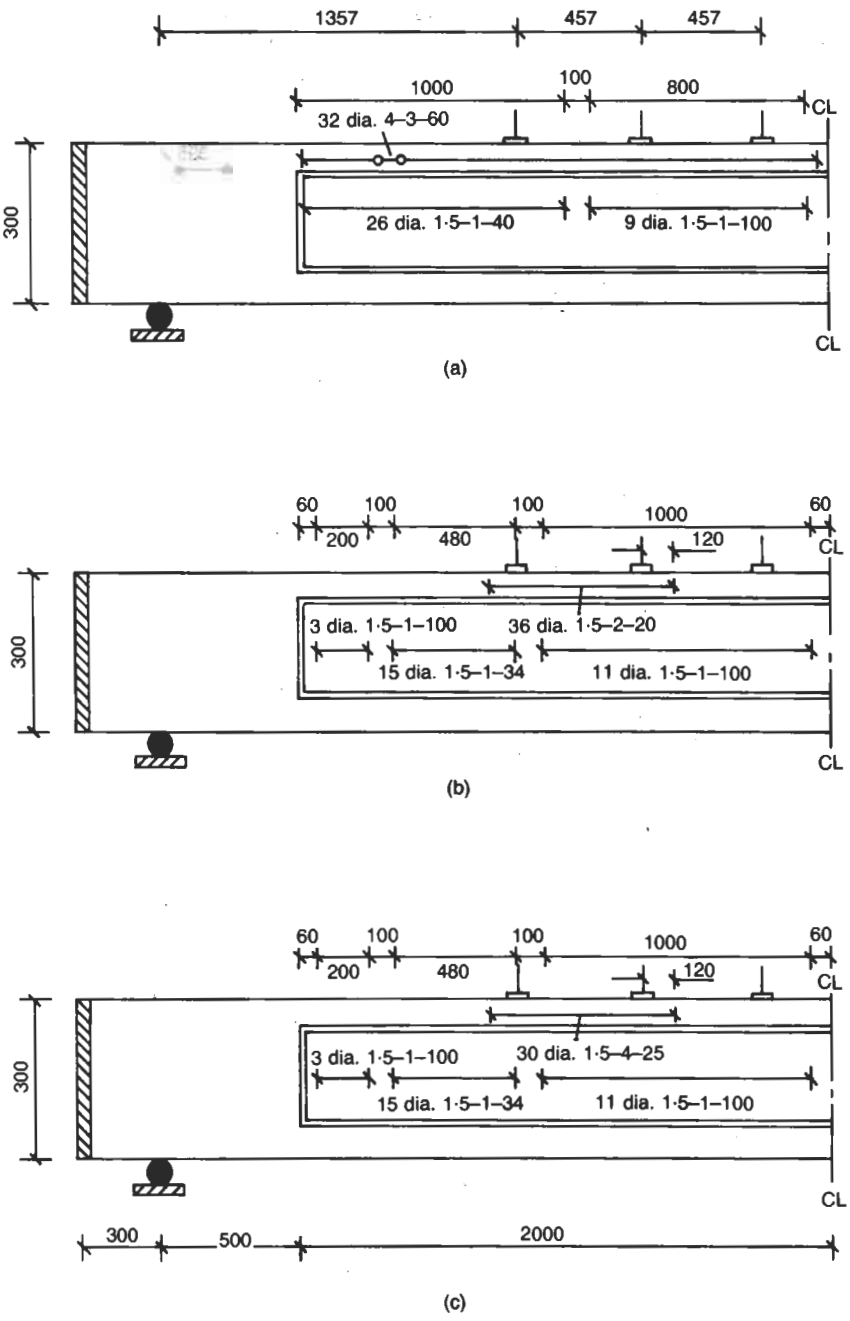

Fig. 9. Transverse reinforcement details of: (a) PCB3; (b) PCB6; (c) PCB7 (all dimensions in mm)

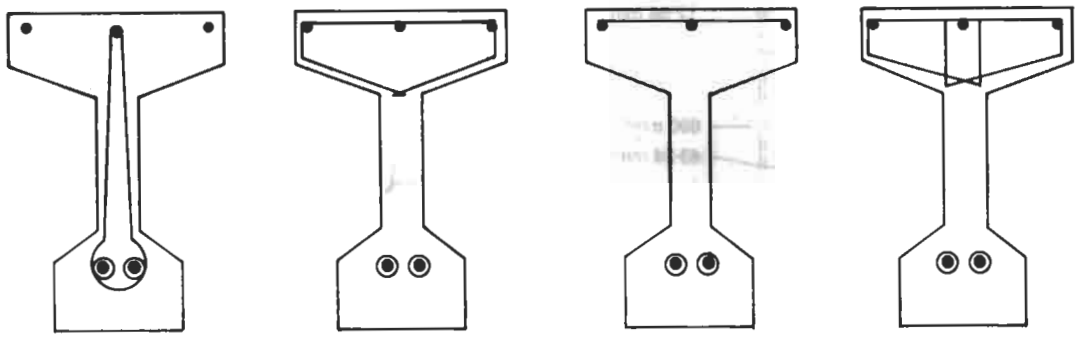

pattern matches quite closely the experimental failure pattern of Fig. 7(a). The analytically-obtained load–deflection curve, although slightly less stiff in the latter stages of loading than the experimental curve, also simulates fairly well the deformational response of the beam.

Case study 3. T-beam PCB3 subjected to six-point loading failing in shear

14. Details of the transverse reinforcement of PCB3 along with those of PCB6 and PCB7 are shown in Fig. 9. These three beams were all subjected to six-point loading. The transverse reinforcement of PCB3, prestressed to an effective prestressing force of about 50·7%, was designed for flexural failure in compliance with the provisions of BS 8110[10] (relevant design calculations are available elsewhere[7]). The f_c value of PCB3 was 46·3 MPa.

15. The FE discretization adopted for the present analysis is shown in Fig. 10, the mesh having 54 HX20 under-integrated brick elements to represent concrete and 164 LM03 bar elements for the steel (considering only one-fourth of the beam). A few minor changes for both the actual dimensions of the span and the position of the loads were introduced in order to use a regular mesh. The half-length of the beam (from the support to the centre-line) in the model was 2513·5 mm instead of the actual dimension of 2500 mm. The overall length of the rectangular block was also reduced; its length overhanging the support was 228·5 mm instead of 300 mm, and the rectangular block from the support up to the beginning of the T-section was 457 mm long instead of the 500 mm used in the experiment. The loading point nearest to the support in the model was located at a distance of 1371 mm instead of 1357 mm; nevertheless, the distance between the load-points both in the analysis and in the experiment was 457 mm. These changes, however, seem to be of only very minor consequence, as the shear forces and bending moments at all the critical sections remain virtually unaffected by such modifications. It can be seen from Fig. 10 that the bottom flange has been modelled by adopting a trapezoidal shape in order to economize in the FE modelling: again, and as reported earlier,[4] this simplification has very little or no impact on the overall prediction of the model, as concrete below the neutral axis plays a much less vital role than widely believed. Fig. 10 also indicates the area of reinforcement of various steel elements of the adopted mesh. All the steel elements were 'smeared' to the adjoining brick-element peripheries. Although the longitudinal top steel was placed at the top edge of the flange, the prestressing steel was smeared in such a manner that both the amount and its centroid remained unchanged. The equivalent area of web and flange steel was calculated and smeared to the abutting brick-element edges in an effort to keep its amount per unit length unchanged. The vertical load was applied to the beam at a rate of about 6·7% of the failure load.

16. Figure 2(c) shows the analytical crack pattern at different load levels up to failure. The MSL in this analysis was 84·17 kN, which is about 92% of the load (including the dead load of the spreader beams) sustained by the beam in the experiment (91·5 kN). The first set of flexural cracks were seen in the midspan and under the innermost loading points at an applied load of 48·10 kN. At a load of 54·11 kN, the number of flexural cracks increased and they entered into the web. Initiation of shear cracks in the web could also be detected at this stage. When the load rose to 60·12 kN, the flexural cracks, formed near the midspan, reached the interface of top flange and web. At the next load step (11), the web of the beam was full of shear cracks. In the subsequent two load steps (12, 13), these shear cracks propagated downwards into the bottom flange and, in addition, the web under the inner loading points became more severely cracked. At the MSL of 84·17 kN, the severity of shear cracking was more pronounced, and one of the cracks, in the midspan of the beam, made its way into the compression flange. Examination of the cracking pattern for load step '777' reveals that, at the point of numerical divergence, quite a number of diagonal cracks actually penetrated into the top flange. At the midspan of the beam, vertical and near horizontal cracks also occurred. It seems that absence of flange reinforcement, in the form of hoops, helped the penetration of the cracks deep into the compression flange, and this, aided by inadequate transverse reinforcement at the CFP-change locations, prompted the beam to sustain a brittle (quasi-ductile) failure. The analytical and experimental load–deflection curves are compared in Fig. 3(c), the former tracing its test counterpart faithfully up to the very last step, when its peak falls just below the experimental value. It is apparent from the above exercise that the experimental findings of PSC beam PCB3 have been adequately simulated by the FE modelling.

Case study 4. T-beam PCB6 subjected to six-point loading failing in flexure

17. The design reinforcement of PCB6, prestressed to an effective prestressing force of about 60%, was provided in compliance with the CFP concept,[11,12] with the relevant calculations for flexural failure available elsewhere.[7] The f_c value for PCB6 was 45·7 MPa.

18. The FE discretization adopted for the analysis of PCB6, consisting of 54 brick elements and 169 bar elements, is identical to that of PCB3 (except for the location of steel elements), which has already been shown in

Fig. 10. The area of transverse reinforcement, of course, has been altered in accordance with the steel requirements for PCB6, as portrayed in Fig. 9(b).

19. The analytical crack patterns at different load levels up to failure appear in Fig. 2(d). The MSL predicted by the analysis was 84·17 kN, which was about 90% of the total load sustained by the beam in the experiment (94 kN). At 60·12 kN, the first set of flexural cracks appeared within the flexural span and below the inner load points. In the subsequent load step, the number of flexural cracks increased. At a load of 72·14 kN, diagonal cracks oriented from the supports to the point loads developed throughout the web of the beam, while the central flexural cracks propagated upwards and reached the intersection of the web and the flange. In the following load step, the number of both flexural and shear cracks grew. When the MSL level was reached, the extension within the top flange of one of the flexural cracks of the flexural span could be seen, and the stress in the prestressing steel at the midspan of the beam passed the yield limit of the tendon. Inspection of the crack pattern at load step 777 reveals that, at failure, some of the flexural cracks in the midspan were greatly widened, as the material at the Gauss points corresponding to those concrete elements collapsed (i.e. third cracking) in the FE analysis. In Fig. 3(d), the applied load is plotted against the midspan deflection, the close agreement between experiment and analysis being apparent. The nature of both the experimental and the analytical curves points to a flexural failure of the beam, the actual ductility being adequately monitored in the analysis. Therefore, it is clear from the above analytical exercise that, on the one hand, the load-carrying capacity, the cracking process and the deformational response of the PSC beam PCB6 have been closely simulated by the adopted FE model, and, on the other hand, provision of localized transverse reinforcement (15 dia. 1·5–1–34 in Fig. 9(b)) at locations where the CFP changes its direction, and additional 'hoop-like' reinforcement (36 dia. 1·5–2—20 in Fig. 9(b)) to prevent bond failure ensure the attainment of a ductile type of failure in a PSC member.

Case study 5. T-beam PCB7 made from HSC subjected to six-point loading failing in flexure

20. Now that the generality of the FE model has been established for both RC and PSC members made from a wide range of concrete strengths, the performance of PSC beams made from HSC can be studied. One such beam, designed to the CFP method (designated as PCB7), is presented in this section. The dimensions and reinforcement details of the beam have already been given in Figs 6 and 9(c) respectively. This beam has been subjected to a similar amount of prestressing force as PCB6 of case study 4. However, unlike the other PSC beams, PCB7 has been designed on the basis of a concrete cube strength of 80 MPa (i.e. f_c = 64 MPa).

21. The FE discretization adopted for the present analysis is the same as the one shown in Fig. 10 (once allowance has been made for the differing steel detailing). The mesh consists of 54 under-integrated brick elements to represent concrete and 174 line elements to depict steel. Once again, while making the necessary alterations in the amount of transverse reinforcement to allow for the actual steel detailing in the beam, all the other simplifications considered for the analysis of PCB6 have also been adopted in the present analysis.

22. Figure 2(e) shows the crack pattern at different load levels up to failure. The MSL predicted by the analysis was 84·17 kN, which was about 88% of the calculated flexural failure load (95·8 kN).[7] It has been observed earlier, during the simulation of PCB3 and PCB6, that, for similar PSC beams, the failure load predicted by the FE model was about 8–10% lower than the experimental failure load. In line with the above observation, it might be argued that, for the present beam, the actual failure load is likely to be proportionately higher (i.e. 88/92 (88/90) × 100 ~96% (98%) of the designed value). The first set of flexural cracks appeared in the midspan of the beam at a load of 60·12 kN. In subsequent load steps, the number of flexural cracks increased, new cracks being formed below the load points. Some of them also propagated upwards and reached the web–flange intersection. It was not until the MSL level that diagonal cracks oriented from the supports to the point loads suddenly developed in the web of the beam. At this stage, one of the midspan flexural cracks penetrated into the flange of the beam and the bottom steel was at yield. The plot of load step 777 shows that, beyond the MSL level, there was no increase in the number of shear cracks. However, a few more flexural cracks entered the top flange of the beam. The applied load has been plotted against midspan deflection in Fig. 3(e). The ductility of the beam at failure is evident from this figure.

23. If the analytical crack patterns of PCB7 (Fig. 2(e)) are compared with those of PCB6 (Fig. 2(d)), it becomes apparent that the formation of shear cracks in PCB7 was much delayed in comparison with PCB6, although the final crack patterns for the two beams are very similar. The finding is in keeping with the observations made elsewhere,[4,13] while comparing the performance of HSC beams with beams made from normal-strength mixes.

24. From the limited information obtained from the above FE modelling, it can tentatively

be concluded that the model for designing PSC members in compliance with the CFP concept can be used in the design of PSC members made from HSC as well.

Conclusions

25. The following main conclusion can be derived from the present study, based on the constant-parameter 3-D FE model for structural concrete described in references 1–3.

26. The FE model under consideration can mimic satisfactorily the experimental load-carrying capacity, deformational response, crack patterns and mode of failure of PSC members, with the effect of prestressing represented simply by inputting the effective prestressing force as a constant load at the first load step and by removing the part of the stress–strain curve of the steel tendon that was effectively utilized in the prestressing operation.

27. It is clear that detailed modelling of the compressive zone of a PSC member is more important than the portion of the member below the neutral axis. Thus, for example, while the imposed additional confinement in the compressive flange of case study 1 increased the load-carrying capacity of the compressive zone of PSC beam CW12 and ultimately caused the attainment of an analytical failure load higher than its experimental counterpart, the slight reduction in the concrete areas of the tensile zone for case studies 2–5 did not have any significant effect.

28. The numerical results obtained from case studies 2–4 have validated the experimental observations that provision of transverse reinforcement complying with the CFP concept results in a safer design solution than that based on current Code tenets. The numerical experiment conducted on a HSC beam designed to the above concept has also shown the suitability of this approach in the design of PSC members made from HSC mixes.

Acknowledgements

29. The first Author expresses his gratitude to the Association of Commonwealth Universities, UK, for awarding him a Commonwealth Scholarship to carry out research of which the present work forms part. Thanks are also due to Bangladesh University of Engineering and Technology for granting him leave of absence during this research programme.

References

1. González Vidosa F. *et al.* A three-dimensional nonlinear finite-element model for structural concrete. Part 1: Main features and objectivity study. *Proc. Instn Civ. Engrs*, Part 2, 1991, **91**, Sept., 517–544. Discussion: *Proc. Instn Civ. Engrs Structs & Bldgs*, 1992, **94**, Aug., 365–374.
2. González Vidosa F. *et al.* A three-dimensional nonlinear finite-element model for structural concrete. Part 2: Generality study. *Proc. Instn Civ. Engrs*, Part 2, 1991, **91**, Sept., 545–560. Discussion: *Proc. Instn Civ. Engrs Structs & Bldgs*, 1992, **94**, Aug., 365–374.
3. González Vidosa F. *et al.* Nonlinear finite-element analysis of concrete structures: Performance of a fully three-dimensional brittle model. *Comp. & Struct.*, 1991, **40**, 5, 1287–1305.
4. Seraj S. M. *et al.* Three-dimensional finite-element modelling of normal- and high-strength reinforced concrete members, with special reference to T-beams. Submitted for publication.
5. Elzanaty A. H. *et al. Shear critical high strength concrete beams*. Department of Structural Engineering, Cornell University, Ithaca, 1985, Research Report No. 85–1.
6. Elzanaty A. H. *et al.* Shear capacity of prestressed concrete beams using high strength concrete. *Am. Concr. Inst. Struct. J.*, 1986, **83**, No. 3, 359–368.
7. Seraj S. M. *Reinforced and prestressed concrete members designed in accordance to the compressive-force path concept and fundamental material properties*. Imperial College, University of London, 1991, PhD thesis.
8. Kotsovos M. D. and Newman J. B. Fracture mechanics and concrete behaviour. *Mag. Concr. Res.*, 1981, **33**, 113, 103–112.
9. Neville A. M. *Properties of Concrete*. Longman Science and Technology, Harlow, 1981, 3rd edn.
10. British Standards Institution. *Code of practice for design and construction*. BSI, London, 1985, BS 8110.
11. Kotsovos M. D. Compressive force path concept: basis for reinforced concrete ultimate limit design. *Am. Concr. Inst. Struct. J.*, 1988, **85**, 1, 68–75.
12. Kotsovos M. D. and Lefas I. D. Behaviour of reinforced concrete beams designed in compliance with the concept of compressive force path. *Am. Concr. Inst. Struct. J.*, 1990, **87**, 2, 127–139.
13. Seraj S. M. *et al.* Behaviour of high-strength mix reinforced concrete beams. Submitted for publication.